

# SWINSRGAN: SWIN TRANSFORMER-BASED GENERATIVE ADVERSARIAL NETWORK FOR HIGH-FIDELITY SPEECH SUPER-RESOLUTION

Jiajun Yuan<sup>1</sup>, Xiaochen Wang<sup>1</sup>, Yuhang Xiao<sup>1</sup>, Yulin Wu<sup>2</sup>, Chenhao Hu<sup>3</sup>, Xueyang Lv<sup>3</sup>

<sup>1</sup> National Engineering Research Center for Multimedia Software,  
School of Computer Science, Wuhan University, Wuhan, China

<sup>2</sup> School of Artificial Intelligence, Jiangnan University, Wuhan, China

<sup>3</sup> Xiaomi Corporation, Beijing, China

E-mails: yjj2002@whu.edu.cn, wuyulin@whu.edu.cn, huchenhao@xiaomi.com

## ABSTRACT

Speech super-resolution (SR) reconstructs high-frequency content from low-resolution speech signals. Existing systems often suffer from representation mismatch in two-stage mel-vocoder pipelines and from over-smoothing of hallucinated high-band content by CNN-only generators. Diffusion and flow models are computationally expensive, and their robustness across domains and sampling rates remains limited. We propose SwinSRGAN, an end-to-end framework operating on Modified Discrete Cosine Transform (MDCT) magnitudes. It is a Swin Transformer-based U-Net that captures long-range spectro-temporal dependencies with a hybrid adversarial scheme combines time-domain MPD/MSD discriminators with a multi-band MDCT discriminator specialized for the high-frequency band. We employ a sparse-aware regularizer on arcsinh-compressed MDCT to better preserve transient components. The system upsamples inputs at various sampling rates to 48 kHz in a single pass and operates in real time. On standard benchmarks, SwinSRGAN reduces objective error and improves ABX preference scores. In zero-shot tests on HiFi-TTS without fine-tuning, it outperforms NVSR and mdctGAN, demonstrating strong generalization across datasets. Samples can be found online<sup>1</sup>.

**Index Terms**— speech super-resolution, bandwidth extension, high-frequency restoration, Swin Transformer, generative adversarial networks

## 1. INTRODUCTION

Speech super-resolution (SR), also known as bandwidth extension, reconstructs a high-resolution signal from a low-resolution input by restoring high-frequency details. This process enhances both perceptual quality and intelligibility, making SR essential for applications such as telecommunications, audio restoration, and text-to-speech synthesis [1, 2, 3]. The task remains highly challenging because speech exhibits fine temporal resolution and complex structures across multiple time scales, requiring models to faithfully capture both short- and long-term dependencies.

Early approaches to bandwidth extension predominantly relied on statistical modeling [4, 5] (e.g., codebook-, HMM-, or GMM-based mapping of spectral envelopes). These methods captured

coarse spectral trends but struggled with nonstationary and long-range spectro-temporal patterns. With the rise of deep learning, non-generative mapping targeted moderate bandwidths (typically up to 16 kHz): AECNN [6] performed waveform-to-waveform regression, and TFNet [7] jointly modeled time and frequency. Optimizing L1/L2 or STFT objectives recovers formants and low-band harmonics, yet treating SR as deterministic regression over-smooths hallucinated high-band content, limiting perceptual sharpness at 48 kHz. To achieve higher perceptual quality and support higher sampling rates, research shifted to generative modeling. Diffusion-based and flow-based approaches (NU-Wave [8], DiffWave [9], WSRGlow [10]) and two-stage pipelines (NVSR [11], AudioSR [12]) leverage strong priors; however, two-stage designs may suffer mel-vocoder representation mismatch and degraded out-of-domain robustness, while diffusion/flow models often incur high computational cost. Building on these foundations, recent advances explore single-step flow matching for efficient generation [13], time-domain SSM-based architectures for end-to-end efficiency [14], and GAN strategies with parallel amplitude-phase prediction [15] or multi-stage sampling control [16]; other lines pursue complex-domain modeling for accurate phase recovery [17] and diffusion-based zero-shot restoration for blind BWE [18].

Motivated by these limitations, vocoder-free SR in an invertible domain avoids the mel-vocoder decoupling. The MDCT-based mdctGAN [19] enables efficient inference on MDCT magnitudes but employs a Pix2Pix-style generator with limited non-local modeling; its arcsinh compression stabilizes training yet suppresses transients, yielding muffled highs and weak band-specific discrimination. In this context, we adopt NVSR and mdctGAN as representative baselines: NVSR typifies strong two-stage mel-vocoder pipelines, and mdctGAN exemplifies vocoder-free, single-stage MDCT-domain modeling; our method leverages their strengths while addressing these limitations.

In this work, we propose SwinSRGAN, a unified end-to-end adversarial framework operating in the MDCT domain. A Swin Transformer-based U-Net generator captures long-range spectro-temporal dependencies while preserving fine-grained details, and a hybrid discriminator integrates time-domain MPD/MSD with a frequency-domain High-Band Multi-Band Discriminator (HB-MBD) to emphasize the reconstructed high-frequency content. The system supports versatile bandwidth extension (from 4-32 kHz to 48 kHz) with real-time inference. Experimental results show consistent improvements over recent speech SR systems on both objective metrics

<sup>1</sup><https://judgelyj.github.io/>

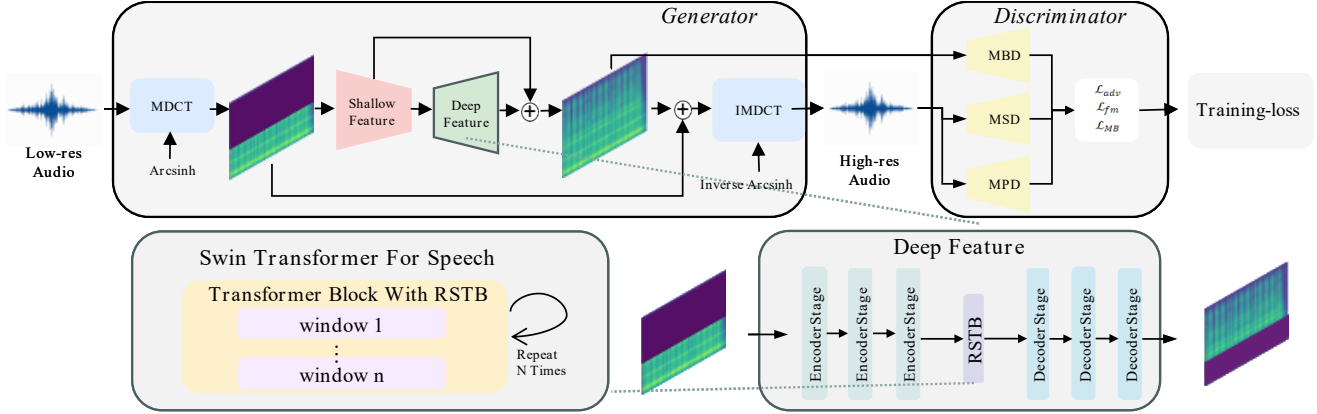


**Fig. 1.** Overall architecture of SwinSRGAN. The generator employs a U-Net architecture with a Swin Transformer backbone. It consists of multiple *Encoder Stages* for downsampling, a central *RSTB* as the bottleneck, and corresponding *Decoder Stages* for upsampling. Crucially, skip connections bridge the encoder and decoder paths to preserve high-fidelity spectral details. The discriminator adopts a hybrid architecture, combining time-domain discriminators (MPD/MSD) with a frequency-domain High-Band Multi-Band Discriminator (HB-MBD) to ensure both temporal coherence and spectral fidelity.

and ABX preference tests. Furthermore, to assess robustness under domain shift, we conduct zero-shot cross-dataset evaluation on HiFi-TTS [20] without fine-tuning; SwinSRGAN consistently achieves lower LSD than NVSR [11] and mdctGAN [19], demonstrating strong generalization beyond the training corpus.

Our main contributions are as follows:

1. An end-to-end MDCT-domain SR framework that eliminates mel-vocoder decoupling while remaining vocoder-free;
2. A Swin Transformer-based U-Net generator that models long-range spectro-temporal dependencies and preserves fine-grained details;
3. A hybrid discriminator incorporating a frequency-domain High-Band Multi-Band Discriminator (HB-MBD) and MPD/MSD, concentrating adversarial pressure on the high-frequency band while maintaining temporal coherence;
4. A sparse-aware regularization tailored to arcsinh-compressed MDCT, enhancing high-band fidelity and mitigating over-smoothing.

## 2. METHOD

SwinSRGAN operates in the MDCT domain and adopts the arcsinh compression used in mdctGAN [19] to stabilize training. However, speech SR requires not only stability but also accurate reconstruction of high-frequency content, which tends to be attenuated by this compression. To address this, we introduce a Swin Transformer-based generator that overcomes the limitations imposed by the inherently local receptive fields of conventional CNNs. Training is guided by a hybrid-domain discriminator that enforces spectral accuracy in the frequency domain and perceptual coherence in the time domain.

In our implementation, we scale the MDCT magnitude  $|X|$  by a gain  $g$  (default  $g=800$ ) and use base-10 scaling for the compression and its exact inversion:

$$\begin{aligned} S &= \operatorname{asinh}(g|X|)/\log(10), \\ |X| &= \sinh(S \log(10))/g. \end{aligned} \quad (1)$$

This choice keeps small values approximately linear while squashing large magnitudes, thereby stabilizing adversarial training.

### 2.1. Swin Transformer-based Speech Generator

Building on this overall framework, we replace the standard convolutional generator with a U-Net architecture incorporating a Swin Transformer backbone, inspired by recent advances in Swin-based restoration [21, 22, 23], as illustrated in Figure 1. This design is tailored to restore fine-grained spectral details and transient information that are often attenuated by arcsinh compression. At its core, the generator consists of multiple Residual Swin Transformer Blocks (RSTBs), which exploit hierarchical attention mechanisms well suited to the anisotropic nature of speech spectrograms. Within each block, the windowed self-attention captures localized harmonic structures, while the shifted-window mechanism models long-range temporal evolution of spectral patterns, such as formant transitions—capabilities beyond simpler CNNs.

We adopt a compact Swin-Base U-Net with RSTBs, skip connections, and a global residual path for high-band residual learning, while shallow convolutions at stage boundaries stabilize optimization. This yields a single-stage, vocoder-free mapping from low- to high-resolution MDCT. Compared with conventional convolutional generators, the Swin Transformer U-Net more effectively captures spectral details and transient cues, leading to refined restoration results.

### 2.2. Hybrid Discriminator

As demonstrated in prior work on generative audio models [24, 25], the design of the discriminator framework is critical for generating high-fidelity waveforms. To ensure temporal coherence, we adopt the proven Multi-Period Discriminator (MPD) and Multi-Scale Discriminator (MSD) from HiFi-GAN [24]. The MPD is effective at capturing different periodic patterns in raw audio, while the MSD operates on downsampled versions of the waveform to evaluate structures at various scales. To address this limitation, we adopt a high-frequency-focused High-Band Multi-Band Discriminator (HB-MBD) that operates on MDCT magnitudes. MDCT coefficients are heavy-tailed and become increasingly sparse with frequency; moreover, the upsampling boundary at  $f_{lo} = (\operatorname{lr\_sr}/\operatorname{hr\_sr}) f_{hi}$  defines a region where all coefficients must be hallucinated. To avoid adversarial signal dilution across the intact low band, we place parallel Patch-

GAN heads only on the added band  $[f_{lo}, f_{hi}]$ , together with a single full-band head for global shape. Bands are split uniformly in Hz (i.e., equal MDCT-bin width) with a minimum number of bins per head to respect the local stationarity of KBD-windowed MDCT tiles. This design concentrates adversarial pressure where it matters, prevents trading quality between sub-bands, and yields crisper harmonics and fricative energy without destabilizing the low band. where  $lr\_sr$  and  $hr\_sr$  denote the input and target sampling rates, respectively;  $f_{hi}$  is the Nyquist frequency at  $hr\_sr$ ; and  $f_{lo}$  is the corresponding upsampling boundary.

### 2.3. Training Loss

We optimize the model with the following combined losses. Experiments use PyTorch [26] on NVIDIA A100, batch size 16, 48,460-sample segments.

**GAN Loss.** We adopt LS-GAN [27] with dual discriminators: a time-domain  $D_{wav}$  (MPD+MSD) and an MDCT-domain HB-MBD  $D_{spec}$ :

$$\begin{aligned}\mathcal{L}_{adv}^{wav}(D_{wav}) &= \mathbb{E}_{(x,s)}[(1 - D_{wav}(x))^2 + (D_{wav}(G(s)))^2] \\ \mathcal{L}_{adv}^{spec}(D_{spec}) &= \mathbb{E}_{(x,s)}[(1 - D_{spec}(S_x))^2 + (D_{spec}(S_{G(s)}))^2] \\ \mathcal{L}_{adv}^{wav}(G) &= \mathbb{E}_s[(1 - D_{wav}(G(s)))^2] \\ \mathcal{L}_{adv}^{spec}(G) &= \mathbb{E}_s[(1 - D_{spec}(S_{G(s)}))^2]\end{aligned}\quad (2)$$

Here,  $x$  and  $s$  denote ground-truth and input;  $D_{wav}$  and  $D_{spec}$  are time- and MDCT-domain discriminators;  $S_x$  and  $S_{G(s)}$  are the corresponding MDCT spectrograms;  $\mathbb{E}[\cdot]$  denotes expectation.

**Feature Matching Loss.** We use feature matching across all discriminator layers to stabilize training [24]:

$$\mathcal{L}_{feat}(G) = \sum_{k=1}^K \mathbb{E}_{(x,s)} \left[ \sum_{l=1}^{L_k} \frac{1}{N_l} \left\| D_k^{(l)}(x) - D_k^{(l)}(G(s)) \right\|_1 \right] \quad (3)$$

where  $K$  is the number of discriminators,  $L_k$  their layer counts,  $N_l$  the elements per feature map;  $D_k^{(l)}(\cdot)$  are layer activations and  $\|\cdot\|_1$  is L1.

**Sparse-Aware Loss.** To mitigate arcsinh-induced smoothing while preserving detail, we use a sparse-aware loss with soft weighting that adapts content vs. sparsity by the ground-truth energy:

$$\begin{aligned}w_c &= \sigma(|S_{hr}| - \tau) \cdot \alpha \\ w_s &= 1 - w_c \\ \mathcal{L}_{sparse}(G) &= \mathbb{E}_{(x,s)} [\lambda_c \cdot w_c \odot \|S_{hr} - \hat{S}_{hr}\|_1 \\ &\quad + \lambda_s \cdot w_s \odot |\hat{S}_{hr}|]\end{aligned}\quad (4)$$

where  $\sigma$  is the sigmoid,  $\tau$  the threshold,  $\alpha$  the steepness;  $w_c, w_s$  are content/sparsity weights;  $S_{hr}, \hat{S}_{hr}$  are target/predicted MDCT magnitudes;  $\odot$  is element-wise;  $\lambda_c, \lambda_s$  are loss weights. This promotes accurate reconstruction in high-energy bins and sparsity elsewhere.

In practice,  $\tau = Q_{0.8}(|S_{hr}|)$  per utterance and frequency bin,  $\alpha = 10$ ,  $\lambda_c = 1.0$ ,  $\lambda_s = 0.25$ ; tuned on a held-out validation set.

We linearly warm up adversarial weights to avoid early instability, letting the generator learn basic reconstruction before full discriminator pressure; this is essential for stable MDCT-domain training.

**Final Objective.** The complete objectives for the generator and discriminators are:

$$\begin{aligned}\mathcal{L}_G &= \lambda_{wav}^{(t)} \mathcal{L}_{adv}^{wav}(G) + \lambda_{spec}^{(t)} \mathcal{L}_{adv}^{spec}(G) + \lambda_{wav} \mathcal{L}_{wav}(G) \\ &\quad + \lambda_{feat} \mathcal{L}_{feat}(G) + \mathcal{L}_{sparse}(G) \\ \mathcal{L}_D &= \mathcal{L}_{adv}^{wav}(D_{wav}) + \mathcal{L}_{adv}^{spec}(D_{spec})\end{aligned}\quad (5)$$

where  $\lambda_{wav}^{(t)}$  and  $\lambda_{spec}^{(t)}$  denote adversarial weights that are linearly warmed up to target values of 0.3 and 0.7, respectively;  $\lambda_{wav} = 5.0$  and  $\lambda_{feat} = 3.0$  are fixed loss weights. Here,  $\mathcal{L}_{wav}$  denotes the multi-resolution STFT reconstruction loss [28], and  $\mathcal{L}_{feat}$  is the feature-matching term. Progressive scheduling is applied to the adversarial terms during the initial 20,000 training steps.

## 3. EXPERIMENTS

### 3.1. Dataset

Our models are trained and evaluated on the VCTK-0.92 corpus [29], which consists of approximately 44 hours of speech from 110 English speakers recorded at 48 kHz. For our experiments, we follow a common data preparation methodology to ensure data quality and consistency [30]. We utilize only the recordings from the `mic1` channel, and exclude speakers `p280` and `p315` due to known recording inconsistencies, a standard practice in studies using this corpus. The remaining 108 speakers are then partitioned into a training set of 100 speakers and a test set comprising the final 8 speakers.

In addition, we adopt the HiFi-TTS corpus [20] as an out-of-domain evaluation set for cross-dataset generalization. HiFi-TTS is a high-fidelity, multi-speaker English dataset containing about 291.6 hours of speech from 10 speakers (at least 17 hours per speaker) sampled at 44.1 kHz, released under the CC BY 4.0 license. For evaluation, we resample the references to 48 kHz to align with our SR pipeline and apply the same bandwidth-simulation protocol as in Section 3.3 to synthesize 4/8/16/24 kHz inputs.

### 3.2. Evaluation Metric

For the objective evaluation of our model’s performance, we utilize the Log-Spectral Distance (LSD) metric [31]. Let  $S$  and  $\tilde{S}$  denote the magnitude spectrograms of the ground-truth and the generated speech signals, respectively. The LSD is defined as follows:

$$\text{LSD}(S, \tilde{S}) = \frac{1}{T} \sum_{t=1}^T \sqrt{\frac{1}{F} \sum_{f=1}^F \left( \log_{10} \frac{S(t, f)^2}{\tilde{S}(t, f)^2} \right)^2} \quad (6)$$

where  $T$  and  $F$  denote the numbers of time frames and frequency bins, respectively, and  $\log_{10}(\cdot)$  is the base-10 logarithm. LSD is a frequency-domain metric that quantifies the logarithmic distance between two magnitude spectra, reported in dB. A lower LSD value indicates a higher perceptual similarity between the two signals, where an LSD of 0 dB signifies that the spectra are identical. The comparative results against baseline systems (WSRGlows [10], NVSR [11], Wave-U-Mamba [14], and mdctGAN [19]) are illustrated in Table 1.

For subjective evaluation, we additionally conduct an ABX listening test: in each trial, listeners are presented with two system outputs (A/B) and a reference X, and asked which of A or B is closer to X. This concise protocol compares perceptual similarity under a shared reference with minimal instruction overhead; aggregated preferences are reported in Figure 3.

### 3.3. Training Details

We synthesize low-resolution inputs on-the-fly by applying a randomized low-pass filter followed by resampling. Concretely, for each training segment sampled at 48 kHz, we randomly draw a target sampling rate  $r \in [4, 32]$  kHz and obtain the input by low-pass filtering and downsampling to  $r$  kHz and then upsampling back to 48 kHz. This dynamic low-pass-and-resample procedure prevents overfitting

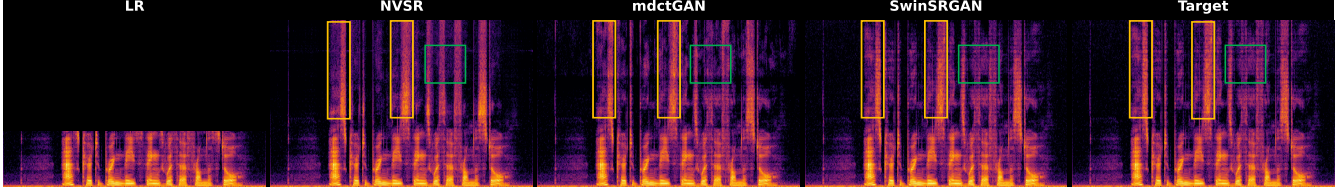


**Fig. 2.** Spectrogram comparison (16kHz→48kHz). SwinSRGAN exhibits sharper harmonic structures, more complete high-band energy, and clearer transients with fewer artifacts, surpassing prior models in both detail and fidelity.

**Table 1.** Objective evaluation results (LSD, dB) and model size (Params, M). Lower LSD is better (The best results have been bolded).

Model	4kHz	8kHz	16kHz	24kHz	AVG	Params
Unprocessed	6.08	5.15	4.85	3.84	4.98	-
WSRGlow	1.12	0.98	0.85	0.79	0.94	229.9M×4
NVSR	0.98	0.91	0.81	0.70	0.85	99.0M
Wave-U-Mamba	0.97	0.87	0.75	0.70	0.82	<b>4.2M</b>
mdctGAN	1.09	0.93	0.83	0.71	0.89	101.0M
<b>SwinSRGAN</b>	<b>0.95</b>	<b>0.84</b>	<b>0.73</b>	<b>0.65</b>	<b>0.79</b>	66.2M
(w/o HB-MBD)	0.99	0.86	0.77	0.71	0.83	-
(w/o Sparse)	0.98	0.85	0.74	0.69	0.81	-

**Table 2.** Cross-dataset generalization on HiFi-TTS (LSD, dB). Lower is better. Zero-shot: no fine-tuning (The best results have been bolded).

Model	4kHz	8kHz	16kHz	24kHz	AVG
NVSR	1.39	1.23	0.93	0.82	1.09
mdctGAN	1.41	<b>1.21</b>	0.95	0.84	1.10
<b>SwinSRGAN</b>	<b>1.33</b>	1.21	<b>0.89</b>	<b>0.78</b>	<b>1.05</b>

to a single cutoff and better matches the evaluation settings with diverse missing bands. Additionally, we apply random segment cropping to ensure consistent training dynamics across diverse acoustic conditions. Unless otherwise stated, the front-end uses MDCT with  $N=1024$  and hop 512 (50% overlap) with a KBD window ( $\alpha=6$ ); the arcsinh gain is set to  $g=800$  by default.

We explored all kinds of Swin backbones and finally adopt *Swin-Base* as our default configuration for SwinSRGAN. Unless otherwise stated, all results reported in this paper for “SwinSRGAN” refer to the Swin-Base variant. We use AdamW with  $\beta_1=0.8$ ,  $\beta_2=0.99$ , and weight decay  $\lambda=0.01$ . The initial learning rate is  $2 \times 10^{-4}$  and decays by a factor of 0.999 at the end of every epoch. The adversarial weights  $\lambda_{wav}^{(t)}$  and  $\lambda_{spec}^{(t)}$  are linearly warmed up to their target values (0.3 and 0.7) over the first 20k steps, consistent with the objective scheduling described in Section 2. All models are trained on a single NVIDIA A100 GPU with a batch size of 16 for 200k steps.

#### 4. RESULTS AND DISCUSSION

For generalization, we assess VCTK-trained models on HiFi-TTS [20] without fine-tuning, synthesizing 4/8/16/24 kHz inputs and computing LSD against 48 kHz references. This zero-shot setting probes cross-dataset robustness under distribution shift. We evaluate each input bandwidth independently and report the mean across them. As summarized in Table 2, SwinSRGAN attains the lowest average

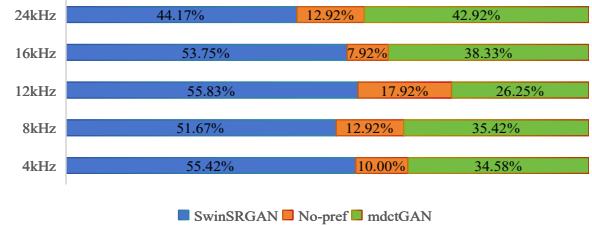


**Fig. 3.** ABX subjective test results of mdctGAN and SwinSRGAN on VCTK test set with 48 kHz target sampling rate.

LSD among the compared methods (NVSR and mdctGAN), with consistent gains across input bandwidths.

For subjective, an ABX test with 12 listeners (20 pairs each); see Figure 3 shows consistent preference for SwinSRGAN over mdctGAN, with the largest margin around 16 kHz and a still favorable outcome at 24 kHz; It shows that the model can maintain high auditory quality while capturing high-frequency details.

For objective, Table 1 reports LSD on VCTK. SwinSRGAN achieves the best average (0.79) with 66.2M parameters, outperforming NVSR (0.85, 99.0M). Ablations confirm complementary gains: removing HB-MBD degrades the average to 0.83, and removing the sparse-aware loss to 0.81. Improvements are largest when the missing band is widest (e.g., 16 kHz→48 kHz), and SwinSRGAN also attains the best 24 kHz score (0.65), indicating a favorable quality–efficiency trade-off relative to heavier diffusion/flow models. Although Wave-U-Mamba [14] uses a much smaller parameter budget, SwinSRGAN remains superior in capturing and reconstructing high-frequency content. (Table 1).

#### 5. CONCLUSIONS

We presented SwinSRGAN, an end-to-end MDCT-domain SR framework with a Swin Transformer U-Net, a time-frequency hybrid discriminator (MPD/MSD + HB-MBD), and a sparse-aware loss. On VCTK, SwinSRGAN attains the best LSD (0.79) with fewer parameters than most baselines, and ABX tests show listener preference over mdctGAN across input rates. These results verify that modeling long-range spectro-temporal dependencies and focusing adversarial pressure on the added high band improve both detail and fidelity. On a single NVIDIA A100 40 GB GPU, 1 s of wall-clock time produces 5.3 s of 48 kHz audio using our model.

#### 6. ACKNOWLEDGMENTS

This work was supported by the National Natural Science Foundation of China under Grant No. 62271358.

## 7. REFERENCES

- [1] S. Chennoukh, A. Gerrits, G. Miet, and R. Sluijter, “Speech enhancement via frequency bandwidth extension using line spectral frequencies,” in *Proc. ICASSP*, 2001, vol. 1, pp. 665–668.
- [2] H. Liu, Q. Kong, Q. Tian, Y. Zhao, D. Wang, C. Huang, and Y. Wang, “Voicefixer: Toward general speech restoration with neural vocoder,” *arXiv preprint arXiv:2109.13731*, 2021.
- [3] K. Nakamura, K. Hashimoto, K. Oura, Y. Nankaku, and K. Tokuda, “A mel-cepstral analysis technique restoring high frequency components from low-sampling-rate speech,” in *Proc. Interspeech*, 2014.
- [4] Y. Cheng, D. O’Shaughnessy, and P. Mermelstein, “Statistical recovery of wideband speech from narrowband speech,” *IEEE Transactions on Speech and Audio Processing*, vol. 2, no. 4, pp. 544–548, 1994.
- [5] Hannu Pulakka, Ulpu Remes, Kalle Palomäki, Mikko Kurimo, and Paavo Alku, “Speech bandwidth extension using gaussian mixture model-based estimation of the highband mel spectrum,” in *Proc. ICASSP*. 2011, pp. 5100–5103, IEEE.
- [6] V. Kuleshov, S. Z. Enam, and S. Ermon, “Audio super resolution using neural networks,” *arXiv preprint arXiv:1703.00841*, 2017.
- [7] Teck Yian Lim, Raymond A. Yeh, Yijia Xu, Minh N. Do, and Mark Hasegawa-Johnson, “Time-frequency networks for audio super-resolution,” in *Proc. ICASSP*, 2018, pp. 646–650.
- [8] J. Lee and S. Han, “Nu-wave: A diffusion probabilistic model for neural audio upsampling,” in *Proc. Interspeech*, 2021, pp. 1634–1638.
- [9] Z. Kong, W. Ping, J. Huang, K. Zhao, and B. Catanzaro, “Dif-flwave: A versatile diffusion model for audio synthesis,” in *Proc. ICLR*, 2021.
- [10] K. Zhang, Y. Ren, C. Xu, and Z. Zhao, “Wsr glow: A glow-based waveform generative model for audio super-resolution,” in *Proc. Interspeech*, 2021, pp. 1649–1653.
- [11] H. Liu, W. Choi, X. Liu, Q. Kong, Q. Tian, and D. Wang, “Neural vocoder is all you need for speech super-resolution,” *arXiv preprint arXiv:2203.14941*, 2022.
- [12] X. Liu, Z. Chen, Y. Liu, J. Li, Z. Wu, H. Liu, Y. Wang, L. Xie, and D. Wang, “Audiosr: Versatile audio super-resolution at scale,” *arXiv preprint arXiv:2305.15733*, 2023.
- [13] Jun-Hak Yun, Seung-Bin Kim, and Seong-Wan Lee, “Flowhigh: Towards efficient and high-quality audio super-resolution with single-step flow matching,” 2025.
- [14] Yongjoon Lee and Chanwoo Kim, “Wave-u-mamba: An end-to-end framework for high-quality and efficient speech super resolution,” 2025.
- [15] Ye-Xin Lu, Yang Ai, Hui-Peng Du, and Zhen-Hua Ling, “Towards high-quality and efficient speech bandwidth extension with parallel amplitude and phase prediction,” 2024.
- [16] Ye-Xin Lu, Yang Ai, Zheng-Yan Sheng, and Zhen-Hua Ling, “Multi-stage speech bandwidth extension with flexible sampling rate control,” 2024.
- [17] Tarikul Islam Tamiti, Biraj Joshi, Rida Hasan, Rashedul Hasan, Taieba Athay, Nursad Mamun, and Anomadarshi Barua, “A high-fidelity speech super resolution network using a complex global attention module with spectro-temporal loss,” 2025.
- [18] Eduard Moliner, Fredrik Elvander, and Vesa Välimäki, “Blind audio bandwidth extension: A diffusion-based zero-shot approach,” *IEEE/ACM Transactions on Audio, Speech, and Language Processing*, vol. 32, 2024.
- [19] C. Shuai, C. Shi, L. Gan, and H. Liu, “mdctgan: Taming transformer-based gan for speech super-resolution with modified dct spectra,” in *Proc. Interspeech*, 2023, pp. 5112–5116.
- [20] Evelina Bakhturina, Vitaly Lavrukhin, Boris Ginsburg, and Yang Zhang, “Hi-fi multi-speaker english tts dataset,” *arXiv preprint arXiv:2104.01497*, 2021.
- [21] Z. Liu, Y. Lin, Y. Cao, H. Hu, Y. Wei, Z. Zhang, S. Lin, and B. Guo, “Swin transformer: Hierarchical vision transformer using shifted windows,” in *Proc. ICCV*, 2021, pp. 10012–10022.
- [22] J. Liang, J. Cao, G. Sun, K. Zhang, L. Van Gool, and R. Timofte, “Swinir: Image restoration using swin transformer,” in *Proc. ICCVW*, 2021, pp. 1833–1844.
- [23] J. Choi, J. Jang, and H. Park, “Swin2sr: Swin2 transformer for compressed image super-resolution and restoration,” *arXiv preprint arXiv:2209.13261*, 2022.
- [24] J. Kong, J. Kim, and J. Bae, “Hifi-gan: Generative adversarial networks for high-fidelity neural vocoder,” in *Proc. NeurIPS*, 2020, pp. 17022–17033.
- [25] K. Kumar, R. Kumar, T. de Boissiere, L. Gestin, W. Z. Teoh, J. Sotelo, A. de Brebisson, Y. Bengio, and A. C. Courville, “Melgan: Generative adversarial networks for conditional waveform synthesis,” in *Proc. NeurIPS*, 2019, pp. 14910–14921.
- [26] A. Paszke et al., “Pytorch: An imperative style, high-performance deep learning library,” in *Proc. NeurIPS*, 2019, pp. 8024–8035.
- [27] X. Mao, Q. Li, H. Xie, R. Y. K. Lau, Z. Wang, and S. Paul, “Least squares generative adversarial networks,” in *Proc. ICCV*, 2017, pp. 2794–2802.
- [28] R. Yamamoto, E. Song, and J. Kim, “Parallel wavegan: A fast waveform generation model,” in *Proc. ICASSP*, 2020, pp. 6174–6178.
- [29] C. Veaux, J. Yamagishi, and K. MacDonald, “Cstr vctk corpus: English multi-speaker corpus for cstr voice cloning toolkit,” 2019.
- [30] C. Wang, S. Wang, Y. Wu, and Z. Liu, “Neural vocoder is all you need for speech enhancement,” *arXiv preprint arXiv:2303.07633*, 2023.
- [31] A. H. Gray, Jr. and J. D. Markel, “Distance measures for speech processing,” *IEEE Transactions on Acoustics, Speech, and Signal Processing*, vol. 24, no. 5, pp. 380–391, 1976.